AGU PUBLICATIONS

Geophysical Research Letters

RESEARCH LETTER
10.1002/2015GL063550

Key Points:
- Greenland flow distortion plays an important role in the climate system
- The resulting weather systems have hitherto unrecognized mesoscale structure
- This mesoscale structure may impact coupled-climate processes in the region

Supporting Information:
- Figures S1–S3

Correspondence to:
G. W. K. Moore,
gwk.moore@utoronto.ca

Citation:
Moore, G. W. K., I. A. Renfrew, B. E. Harden, and S. H. Mernild (2015), The impact of resolution on the representation of southeast Greenland barrier winds and katabatic flows, *Geophys. Res. Lett.*, *42*, 3011–3018, doi:10.1002/2015GL063550.

Received 18 FEB 2015
Accepted 19 MAR 2015
Accepted article online 24 MAR 2015
Published online 19 APR 2015

The impact of resolution on the representation of southeast Greenland barrier winds and katabatic flows

G. W. K. Moore[1], I. A. Renfrew[2], B. E. Harden[3], and S. H. Mernild[4]

[1]Department of Physics, University of Toronto, Toronto, Ontario, Canada, [2]Centre for Ocean and Atmospheric Sciences, School of Environmental Sciences, University of East Anglia, Norwich, UK, [3]Department of Physical Oceanography, Woods Hole Oceanographic Institution, Woods Hole, Massachusetts, USA, [4]Center for Scientific Studies/Centro de Estudios Cientificos, Validivia, Chile

Abstract Southern Greenland is characterized by a number of low-level high wind speed weather systems that are the result of topographic flow distortion. These systems include barrier winds and katabatic flow that occur along its southeast coast. Global atmospheric reanalyses have proven to be important tools in furthering our understanding of these orographic winds and their role in the climate system. However, there is evidence that the mesoscale characteristics of these systems may be missed in these global products. Here we show that the Arctic System Reanalysis, a higher-resolution regional reanalysis, is able to capture mesoscale features of barrier winds and katabatic flow that are missed or underrepresented in ERA-I, a leading modern global reanalysis. This suggests that our understanding of the impact of these wind systems on the coupled-climate system can be enhanced through the use of higher-resolution regional reanalyses or model data.

1. Introduction

Moore and Renfrew [2005] used scatterometer winds to show that the southeast coast of Greenland was a region where high wind speed flow parallel to the coast frequently occurred and argued it was due to barrier flow. In addition, they identified two local maxima in the occurrence frequency of barrier winds along the Denmark Strait (please refer to Figure S1 in the supporting information for locations of interest described in this paper). *Harden and Renfrew* [2012] and *Moore* [2012] noted that these two maxima were collocated with steep coastal topography. Furthermore, *Harden and Renfrew* [2012] used idealized model simulations to argue that the enhanced wind speeds were the result of cross-isobar acceleration arising from the flow impinging on these topographic barriers as well as downslope acceleration through the excitation of mountain waves. Southeast Greenland also experiences strong katabatic wind events that are channeled into the region's large fjords resulting in strong northwesterly flow known locally as *piteraqs* [*Rasmussen*, 1989; *Oltmanns et al.*, 2014].

These winds play an important role in the regional weather [*Rasmussen*, 1989; *Renfrew et al.*, 2008; *Oltmanns et al.*, 2014]. In addition, the elevated air-sea fluxes of heat, moisture, and momentum associated with these winds impact the regional oceanography [*Haine et al.*, 2009; *Harden et al.*, 2014a]. Furthermore, *Straneo et al.* [2010] argued that barrier flow is important in the exchange of water between fjords and the open ocean along the southeast coast of Greenland. These strong downslope wind events can also result in the removal of a fjord's ice mélange, a mixture of sea ice and icebergs that inhibits glacier calving, thereby contributing to the destabilization of glaciers in the region [*Oltmanns et al.*, 2014].

Southeast Greenland is a data sparse region, making it a challenge to investigate the structure and dynamics of these winds as well as their climate impacts. Reanalyses provide a representation of the atmosphere that is suitable for studying these systems [*Moore*, 2003; *Våge et al.*, 2009; *Harden et al.*, 2011; *Moore*, 2012; *Oltmanns et al.*, 2014]. However, these weather systems are mesoscale phenomena that have horizontal length scales on the order of 200 km [*Heinemann and Klein*, 2002; *Moore and Renfrew*, 2005; *Petersen et al.*, 2009]. As a consequence, they may be underresolved in current global reanalysis products that typically have effective horizontal resolutions on the order of 400 km or greater, i.e., 5–7 times the grid size [*Skamarock*, 2004; *Condron and Renfrew*, 2013].

As a consequence, there is a need to develop climatologies of these topographic weather systems that captures their mesoscale structure. The recent completion of the Arctic System Reanalysis (ASR) [*Bromwich et al.*, 2015] offers the possibility of achieving this goal. The ASR used the Polar Weather Research and Forecasting (WRF)

Table 1. Comparison of Observed and Reanalysis Winds at Stations in the Vicinity of the Sermilik and Køge Bugt Fjords During the Winter Months (December-January-February, DJF) 2000–2012[a]

	Tasiilaq (65°36′N, 37°37′W)		Coast Station (65°40.8′N, 37°55′W)		Ikermit (64°47′N, 40°18′W)	
	Wind Speed	Wind Direction	Wind Speed	Wind Direction	Wind Speed	Wind Direction
Observations	mean = 4.8 m/s	mean = 7°	mean = 6.7 m/s	mean = 37°	mean = 10.2 m/s	mean = 328°
ERA-I	mean = 7.7 m/s	mean = 38°	mean = 6.4 m/s	mean = 27°	mean = 7.8 m/s	mean = 347°
	$r = 0.53$	$r = 0.68$	$r = 0.22$	$r = 0.59$	$r = 0.73$	$r = 0.95$
	rmse = 4.6 m/s	rmse = 99°	rmse = 4.1 m/s	rmse = 63°	rmse = 5.1 m/s	rmse = 49°
ASR	mean = 8.3 m/s	mean = 57°	mean = 6.5 m/s	mean = 42°	mean = 7.8 m/s	mean = 347°
	$r = 0.52$	$r = 0.77$	$r = 0.23$	$r = 0.48$	$r = 0.84$	$r = 0.97$
	rmse = 6.8 m/s	rmse = 79°	rmse = 5.9 m/s	rmse =78°	rmse = 4.3 m/s	rmse = 37°

[a]For the observed and reanalysis winds, the mean wind speed and direction are shown. Also shown are the correlation coefficient (r) and root-mean-square error (rmse) between the observed and reanalysis wind speed and direction.

numerical weather prediction system to generate a regional reanalysis of the Arctic for the period 2000–2012 with a horizontal grid resolution of 30 km. Polar WRF contains a number of modifications to the standard Weather Research and Forecasting (WRF) model that are optimized for use in polar regions [*Hines et al*., 2011]. A comparison using data from middle and high latitudes of the Northern Hemisphere for a 1 year period indicated that the annual mean biases in surface and 500 mb meteorological fields in the Interim Reanalysis from the European Center for Medium-Range Forecasts (ERA-I) [*Dee et al*., 2011] and ASR are comparable, but that the ASR typically has smaller root-mean-square errors and higher correlations [*Bromwich et al*., 2015].

In this paper, we will compare and contrast the representation of barrier winds and katabatic flow along the southeast coast of Greenland in the ERA-I with that from the ASR. The higher horizontal resolution of the ASR allows it to better define the topography including an improved representation of the ridges known as the Watkins Range and Schweizer Land that are situated between southeast Greenland's major fjords as well as the topographic gradient along the margin of the inland ice (Figure S1 in the supporting information).

2. Observations

Figure S2 shows the topography in the immediate vicinity of the Sermilik and Køge Bugt Fjords, a region along Greenland's southeast coast that is relatively well instrumented with three automatic weather stations. There are two Danish Meteorological Institute (DMI) stations; one is situated outside of the Sermilik Fjord in the town of Tasiilaq, while the other at Ikermit is situated offshore of the Køge Bugt Fjord [*Carstensen and Jørgensen*, 2010]. In addition, the Coast Station is situated within the Sermilik Fjord [*Mernild et al*., 2008]. As a consequence of the complex topography in the region, the wind regimes at the three stations are quite different (Figure S3). Even though the Coast Station is only 16 km from Tasiilaq, it experiences a higher mean wind speed, 5.2 m/s versus 2.6 m/s, and directional constancy, 0.74 versus 0.23, during the winter [*Oltmanns et al*., 2014]. Indeed, the correlation between the wind speed during the winter at these two sites is ~0.4, a value similar to that between the two DMI stations that are ~160 km apart.

Table 1 shows the correlation coefficients and root-mean-square errors between the observations and the two reanalyses for the wind speed and direction at the three sites during the winter. At Tasiilaq and Coast Station, neither reanalysis is able to capture the observed variability. This is not unexpected given the different wind regimes, as noted above, at these two nearby sites. The situation is quite different at Ikermit where both reanalyses are able to better capture the temporal variability in wind speed and direction. The location of this station, on an island away from the Greenland coast, contributes to the improved representation of the wind field. However, the ASR has higher correlations and lower root-mean-square errors as compared to the ERA-I at this station.

3. Results

With the caveat that variability of the wind field in regions of complex topography may not be fully captured in either reanalysis, we present in Figure 1 the winter climatological 10 m wind speed in southeast Greenland from the two reanalyses. The ERA-I has a broad region of low wind speed that extends southward from the

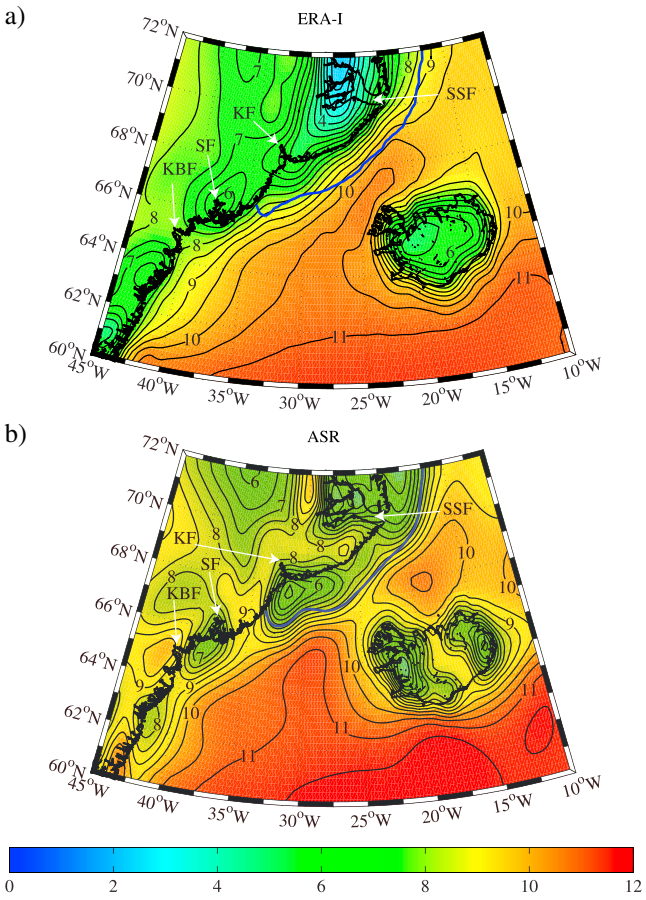

Figure 1. The winter mean (DJF) 10 m wind speed (contours and shading: m/s) fields as depicted in the (a) ERA-I and (b) ASR for the period 2000–2012. The thick blue contour represents the 50% sea ice contour in the respective reanalysis. The four main fjords in the region, the Køge Bugt Fjord (KBF), the Sermilik Fjord (SF), the Kangerdlugssuaq Fjord (KF), and the Scoresby Sund Fjord (SSF), are indicated.

Scoresby Sund Fjord to the Kangerdlugssuaq Fjord as well as another local minimum in the vicinity of the Sermilik Fjord. In the ASR, the northern feature is separated into two distinct minima that are separated by a region of higher wind speed along the ridge between the two fjords. In addition, the minima in the ASR associated with the Sermilik and Kangerdlugssuaq Fjords extend offshore, suggesting that there is some sheltering by the upwind topography. The ASR has a local maximum in the 10 m wind speed inland of the Køge Bugt Fjord that is absent from the ERA-I. Both reanalyses have a gradient in wind speed across the marginal ice zone that is most likely the result of the rougher surface of the sea ice as compared to the open ocean [*Liu et al*., 2006; *Petersen and Renfrew*, 2009]. In the ASR, the gradient is stronger, perhaps as a result of its higher resolution or a different surface exchange parameterization. The wind speed in the vicinity of the Denmark Strait is also different with the ASR indicating the presence of a saddle point in the center of the strait that may be the result of an improved representation of the topographic flow distortion around Iceland's Westfiords Peninsula. Indeed, the ASR has more detail regarding the 10 m wind field around Iceland as compared to the ERA-I.

The ability of the ASR to represent mesoscale flow features is confirmed in Figure 2, which shows the power spectrum of the 10 m wind speed as represented in the two reanalyses. Spectra were calculated along every longitudinal section in Figure 1 during the winter months 2000–2012 for each reanalysis and then averaged over latitude and time. Also shown are spectra characteristic of 3-D turbulence [*Skamarock*, 2004] and midlatitude scatterometer winds [*Patoux and Brown*, 2001]. As discussed by previous authors [*Condron and Renfrew*, 2013; *Moore*, 2014], the ERA-I has reduced power and a steeper slope as compared to the 3-D turbulence and scatterometer spectra at length scales below its effective horizontal resolution of ~400 km

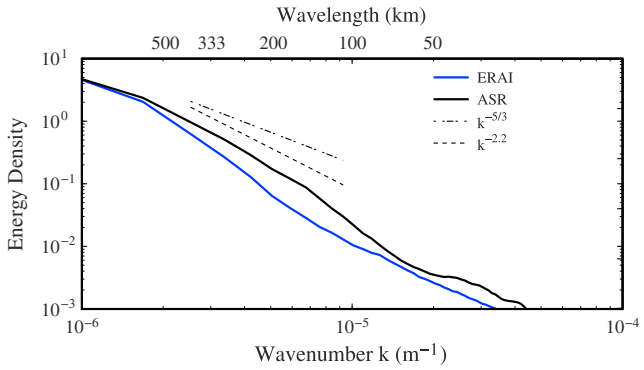

Figure 2. Power spectra of the 10 m wind speed in the vicinity of southeast Greenland. The black line shows the spectrum for the ASR winds, while the blue line shows that for the ERA-I winds. The spectra are averages over the domain of Figure 1 for the months of December, January, and February during 2000–2012. Also shown are spectra representative of 3-D turbulence ($k^{-5/3}$) and scatterometer winds ($k^{-2.2}$).

[*Skamarock*, 2004]. Between wavelengths of 150 and 400 km, the ASR has more power and a slope that approximates that of the 3-D turbulence and scatterometer spectra, implying its effective resolution is ~150 km.

Figure 3 shows the occurrence frequency of high speed northeasterly (barrier) flow and northwesterly (katabatic) flow during the winter as represented in the ERA-I and ASR. The threshold criterion for northeasterly flow was set at 15 m/s, while that for northwesterly flow was set at 12 m/s. Other criteria produced similar results.

With regard to barrier flow (Figures 3a and 3b), both reanalyses capture the two Denmark Strait locations where high speed winds are observed in QuikSCAT data [*Moore and Renfrew*, 2005]. As discussed by previous authors [*Harden and Renfrew*, 2012; *Moore*, 2012], the northern location is in the vicinity of the steep ridge associated with the Watkins Range, while the southern location is in the vicinity of the high topography of Schweizer Land. In addition, the northern maximum in the ASR is located over the open water with an enhanced gradient along the ice edge as well as an extension inland over the steep topography of the Watkins Range, while this maximum is more diffuse in the ERA-I. The ASR occurrence frequency in the southern location has a pronounced inland extension over the steep coastal topography to the north of Sermilik Fjord that is absent in the ERA-I.

Considering northwesterly flow, one again sees that there is more detail in the ASR (Figure 3d) as compared to that from the ERA-I (Figure 3c). In general, the occurrence frequencies for northwesterly flow in the ASR are higher than those in the ERA-I. Along the steep topographic gradient to the east of the North Dome, the ERA-I has a meridionally oriented region where there is an elevated occurrence frequency for northwesterly flow. The feature extends southward to the Kangerdlugssuaq Fjord. In the ASR, this feature is broken into two distinct segments by the topography of Watkins Land. Both reanalyses indicate that the highest occurrence frequency for katabatic flow occurs in the vicinity of the Køge Bugt Fjord. The ASR indicates that there is an offshore extension of the maximum in occurrence frequency that is muted in the ERA-I.

To elucidate the structure of barrier wind and katabatic flow in the two reanalyses, winter events during which high speed northeasterly (barrier) flow was observed at Tasiilaq in addition to those during which high speed northwesterly (katabatic) flow occurred at the Coast Station were identified. Based on the 95th percentile wind speed at the two sites, cutoffs of 10 m/s and 15 m/s were respectively used to identify events. A manual inspection of the AWS data identified distinct events that were separated from each other by at least 24 h. In addition, the Coast Station wind rose (Figure S3) indicated the prevalence of northerly wind events and so the criterion for northwesterly flow was adjusted to include events where the wind direction was between 270° and 10°. With this approach, 50 barrier and 21 katabatic wind events were identified during the period 2000–2012. For the ERA-I compositing, the time of the events was rounded to the nearest 6-hourly time, while for the ASR the rounding was to the nearest 3-hourly time. No appreciable difference in the ASR composites was noted if the rounding was to the nearest 6-hourly time.

Figure 4 shows the composite 10 m wind fields for both classes of events as represented in the two reanalyses. With respect to the northeasterly events, the ASR (Figure 4b) is able to capture the high wind speeds over the steep coastal topography that have been proposed to be the result of downslope acceleration associated with mountain waves [*Harden and Renfrew*, 2012]. This feature is absent in the ERA-I composite. As a result, the 10 m wind speeds in the vicinity of the Sermilik Fjord are higher in the ASR composite as compared to those in the ERA-I composite (Figure 4a). At Tasiilaq, the observed composite wind speed during these events was 13.3 m/s, while in the ERA-I and ASR it was 16.9 and 21.2 m/s, respectively. By not resolving the downslope

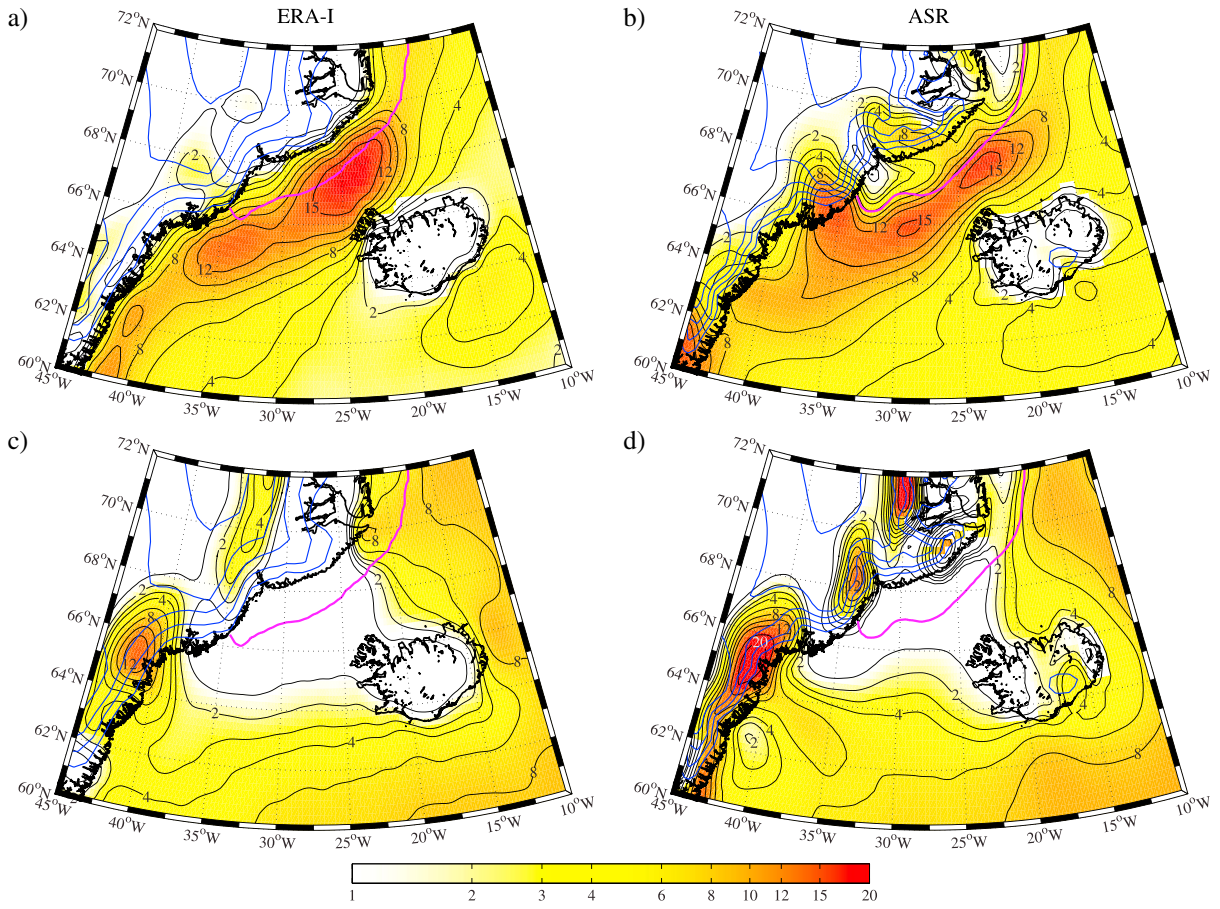

Figure 3. The frequency of occurrence (%) of northeasterly 10 m winds in excess of 15 m/s during the winter (DJF) 2000–2012 as represented in the (a) ERA-I and (b) ASR. The frequency of occurrence (%) of northwesterly 10 m winds in excess of 12 m/s during the winter (DJF) 2000–2012 as represented in the (c) ERA-I and (d) ASR. The thick pink line represents the winter mean 50% sea ice concentration contour in the respective reanalyses. The thick blue lines represent the 500, 1000, 1500, 2500, and 3000 height contours in the respective reanalyses.

acceleration, the ERA-I is, paradoxically, in better agreement with the observations. It is possible that there is some sheltering by the complex topography in the region, unresolved in the ASR, that results in the low wind speeds at Tasiilaq during barrier wind events. The dramatic difference in the wind climate at Tasiilaq and Coast Station, stations that are only 16 km apart, is consistent with this interpretation.

With respect to the northwesterly events, both the ERA-I (Figure 4c) and ASR (Figure 4d) composites indicate that the highest wind speeds during outflow events within the Sermilik Fjord occur in the vicinity of the Køge Bugt Fjord where the maximum wind speed for these events was larger in the ASR, ~20 m/s, as compared to the ERA-I, ~16 m/s. The ASR places the maximum in the vicinity of the steep topography inland of the fjord, while the maximum is more diffuse in the ERA-I. The ASR also has a jet-like extension of the region of high wind speed over the ocean that is muted in the ERA-I.

4. Discussion

Barrier winds and katabatic flows that occur in southeast Greenland play an important role in the regional weather and climate. The data sparse nature of the region makes it a challenge to observe them, and as a result, atmospheric reanalyses have played a crucial role in their characterization. We have shown that a higher-resolution regional reanalysis exhibits more mesoscale variability as compared to a typical global reanalysis. This is likely to impact how we view the role of these orographic winds in the climate system.

Harden and Renfrew [2012] proposed that the excitation of mountain waves along the steep topographic ridges of southeast Greenland during barrier wind events could result in a downslope acceleration of the

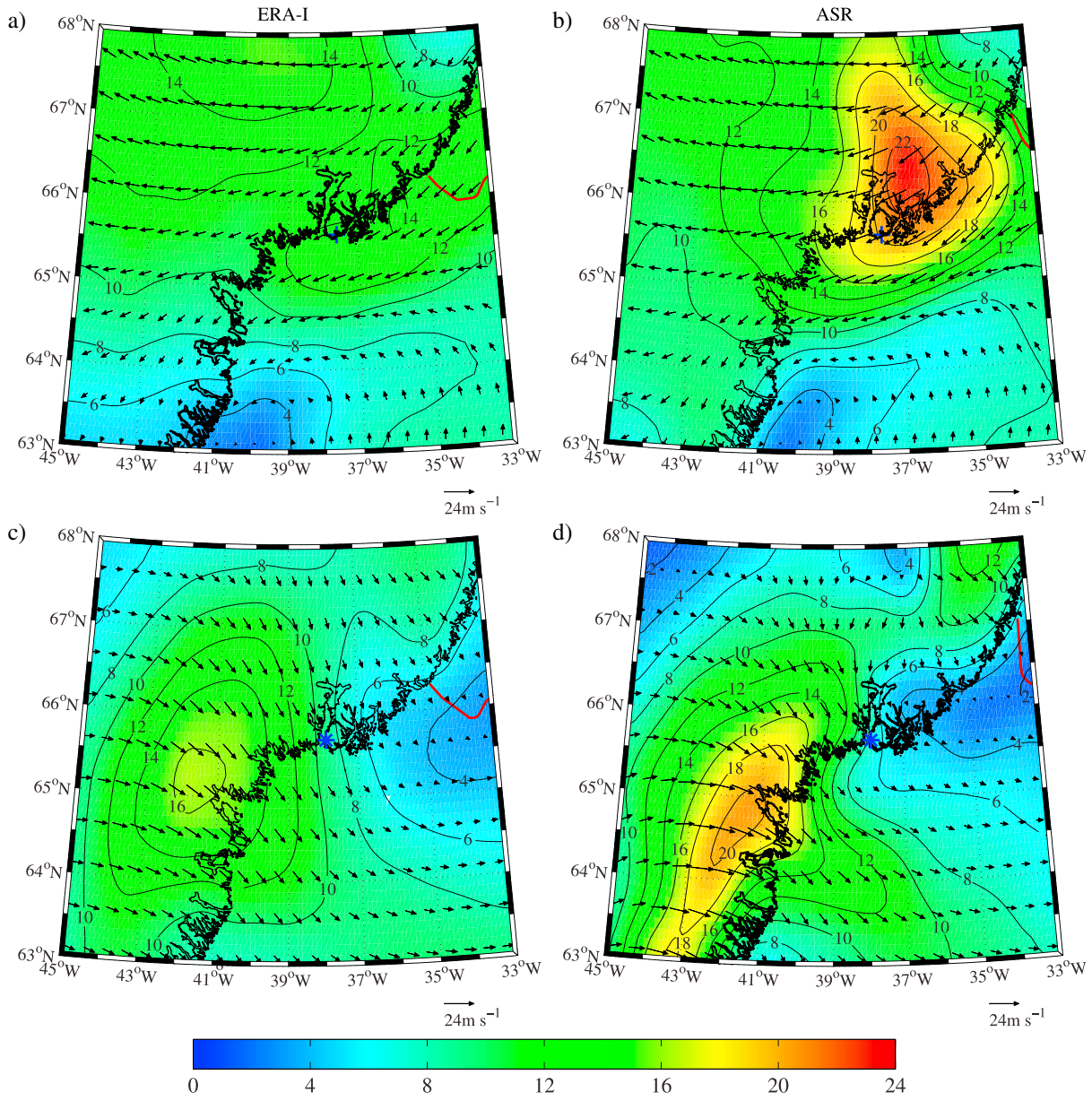

Figure 4. The composite 10 m wind (m/s: vectors) and 10 m wind speed (m/s: contours and shading) of northeasterly wind events at Tasiilaq (denoted by the blue cross) that exceed 15 m/s during the winter (DJF) 2000–2012 as represented in the (a) ERA-I and (b) ASR. The composite 10 m wind (m/s: vectors) and 10 m wind speed (m/s: contours and shading) of northwesterly wind events at Coast Station (denoted by the blue asterisk) that exceed 10 m/s during the winter (DJF) 2000–2012 as represented in the (c) ERA-I and (d) ASR. The thick red lines represent the composite 50% sea ice concentration contour in the respective reanalysis.

wind. The composite barrier flow event considered here had a markedly different structure in the two reanalyses, with the ASR composite containing a region of high surface wind speed along the topography to the north of the Sermilik Fjord—a feature that was absent from the ERA-I composite. We propose that this region of high wind speed is a signature of downslope wind acceleration providing a confirmation of the dynamics proposed by *Harden and Renfrew* [2012].

As a result, wind speeds over the ocean in the vicinity of the Sermilik Fjord are higher in the ASR composite as compared to those in the ERA-I. If confirmed, this shift in strength and dynamics of the wind maximum associated with barrier flow should yield new insight into the location and strength of ocean forcing that occurs along the southeast coast. This would aid the development of ideas surrounding downwelling [*Harden et al.*, 2014a] and fjord-shelf exchange [*Straneo et al.*, 2010; *Harden et al.*, 2014b] that have currently been developed in the absence of such high-resolution atmospheric reanalysis.

The interaction of katabatic flow with the major fjord systems in the region can result in high-speed outflow events or *piteraqs*. The focus of interest with respect to these events in southeast Greenland has been in the vicinity of the Sermilik and Kangerdlugssuaq Fjords, where historical records and observations exist [*Manley*, 1938; *Rasmussen*, 1989; *Mernild et al*., 2008; *van As et al*., 2014]. The results presented in this paper indicate that in both the ERA-I and ASR, the highest occurrence frequency of these events occurs in the vicinity of the Køge Bugt Fjord. This fjord's outlet glaciers have also recently undergone retreats [*Murray et al*., 2010]. However, the role that katabatic flow may have played in this change has not been investigated. Although *Oltmanns et al*. [2015] showed that even a horizontal resolution of 30 km is still insufficient to fully resolve katabatic flow in this region, a move toward a higher-resolution reanalysis is clearly vital to examine the role these winds play in driving long-term changes to the Greenland's marine-terminating glaciers.

The results presented suggest that some of the very intense *piteraqs* observed in the vicinity of Sermilik Fjord may have been stronger farther to the south near the Køge Bugt Fjord. In addition, the wind speeds in the ASR composite katabatic flow event were higher and more tightly focused in the region of steep coastal topography inland of this fjord than was the case for the ERA-I composite. This may be the result of the ASR's enhanced ability to resolve the downslope acceleration associated with breaking mountain waves as compared to the ERA-I [*Doyle et al*., 2005; *Oltmanns et al*., 2014]. Support for this idea comes from *Moore* [2013] who used an interim version of the ASR to show that high surface wind speeds in the lee of Novaya Zemlya were the result of downslope winds resulting from the critical level absorption of mountain waves.

The results presented in this paper suggest that the ASR is able to more fully resolve the mesoscale structure of these wind systems thereby improving our ability to characterize their climate impact. However, there are likely features of these wind systems that are not resolved by the ASR. An example is the mismatch between the wind speed observed at Tasiilaq during barrier wind events with that in the ASR. In addition, caution must be expressed because many features of these weather systems are strongly influenced by the parameterizations that are part of the underlying numerical models and that without a control for these influences, it is a challenge to assess the improvement in the representation of these weather systems that arises from increased horizontal resolution alone.

Acknowledgments

The ERA-I reanalysis fields are available from the ECMWF (www.ecmwf.int), the ASR reanalysis fields are available from NCAR (www.rda.ucar.edu), and the weather station data are available from the DMI (www.dmi.dk) and S. Mernild.

The Editor thanks two anonymous reviewers for their assistance in evaluating this paper.

References

Bromwich, D. H., A. B. Wilson, L. Bai, G. E. K. Moore, and P. Bauer (2015), Contrasting the regional Arctic System Reanalysis with the global ERA-Interim Reanalysis, *Q. J. R. Meteorol. Soc.*, doi:10.1002/qj.2527, in press.

Carstensen, L. S., and B. V. Jørgensen (2010), Weather and climate data from Greenland 1958–2009 Rep, Danish Meteorological Institute.

Condron, A., and I. A. Renfrew (2013), The impact of polar mesoscale storms on northeast Atlantic Ocean circulation, *Nat. Geosci.*, *6*(1), 34–37.

Dee, D. P., et al. (2011), The ERA-Interim Reanalysis: Configuration and performance of the data assimilation system, *Q. J. R. Meteorol. Soc.*, *137*(656), 553–597.

Doyle, J. D., M. A. Shapiro, Q. Jiang, and D. L. Bartels (2005), Large-amplitude mountain wave breaking over Greenland, *J. Atmos. Sci.*, *62*(9), 3106–3126.

Haine, T. W. N., S. Zhang, G. W. K. Moore, and I. A. Renfrew (2009), On the impact of high-resolution, high-frequency meteorological forcing on Denmark Strait ocean circulation, *Q. J. R. Meteorol. Soc.*, *135*(645), 2067–2085.

Harden, B. E., and I. A. Renfrew (2012), On the spatial distribution of high winds off southeast Greenland, *Geophys. Res. Lett.*, *39*, L14806, doi:10.1029/2012GL052245.

Harden, B. E., I. A. Renfrew, and G. N. Petersen (2011), A climatology of wintertime barrier winds off southeast Greenland, *J. Clim.*, *24*(17), 4701–4717.

Harden, B. E., R. S. Pickart, and I. A. Renfrew (2014a), Offshore transport of dense water from the east Greenland Shelf, *J. Phys. Oceanogr.*, *44*(1), 229–245.

Harden, B. E., F. Straneo, and D. A. Sutherland (2014b), Moored observations of synoptic and seasonal variability in the east Greenland Coastal Current, *J. Geophys. Res. Oceans*, *119*(12), 8838–8857, doi:10.1002/2014JC010134.

Heinemann, G., and T. Klein (2002), Modelling and observations of the katabatic flow dynamics over Greenland, *Tellus Ser. A-Dyn. Meteorol. Ocean.*, *54*(5), 542–554.

Hines, K. M., D. H. Bromwich, L.-S. Bai, M. Barlage, and A. G. Slater (2011), Development and testing of Polar WRF. Part III: Arctic land, *J. Clim.*, *24*(1), 26–48.

Liu, A. Q., G. W. K. Moore, K. Tsuboki, and I. A. Renfrew (2006), The effect of the sea-ice zone on the development of boundary-layer roll clouds during cold air outbreaks, *Boundary-Layer Meteorol.*, *118*(3), 557–581.

Manley, G. (1938), Meteorological observations of the British East Greenland expedition, 1935–36, at Kangerdlugssua, 68° 10′N, 31° 44′W, *Q. J. R. Meteorol. Soc.*, *64*(275), 253–276.

Mernild, S. H., B. U. Hansen, B. H. Jakobsen, and B. Hasholt (2008), Climatic conditions at the Mittivakkat Glacier catchment (1994–2006), Ammassalik Island, SE Greenland, and in a 109-year perspective (1898–2006), *Geografisk Tidsskrift-Dan. J. Geogr.*, *108*(1), 51–72.

Moore, G. W. K. (2003), Gale force winds over the Irminger Sea to the east of Cape Farewell, Greenland, *Geophys. Res. Lett.*, *30*(17), 1894, doi:10.1029/2003GL018012.

Moore, G. W. K. (2012), A new look at Greenland flow distortion and its impact on barrier flow, tip jets and coastal oceanography, *Geophys. Res. Lett.*, *39*, L22806, doi:10.1029/2012GL054017.

Moore, G. W. K. (2013), The Novaya Zemlya Bora and its impact on Barents Sea air-sea interaction, *Geophys. Res. Lett.*, *40*(13), 3462–3467, doi:10.1002/grl.50641.
Moore, G. W. K. (2014), Mesoscale structure of Cape Farewell tip jets, *J. Clim.*, *27*(23), 8956–8965.
Moore, G. W. K., and I. A. Renfrew (2005), Tip jets and barrier winds: A QuikSCAT climatology of high wind speed events around Greenland, *J. Clim.*, *18*(18), 3713–3725.
Murray, T., et al. (2010), Ocean regulation hypothesis for glacier dynamics in southeast Greenland and implications for ice sheet mass changes, *J. Geophys. Res.*, *115*, F03026, doi:10.1029/2009JF001522.
Oltmanns, M., F. Straneo, G. W. K. Moore, and S. H. Mernild (2014), Strong downslope wind events in Ammassalik, southeast Greenland, *J. Clim.*, *27*(3), 977–993.
Oltmanns, M., F. Straneo, H. Seo, and G. W. K. Moore (2015), The role of wave dynamics and small-scale topography for downslope wind events in southeast Greenland, *J. Atmos. Sci.*, in press.
Patoux, J., and R. A. Brown (2001), Spectral analysis of QuikSCAT surface winds and two-dimensional turbulence, *J. Geophys. Res.*, *106*(D20), 23,995–24,005, doi:10.1029/2000JD000027.
Petersen, G. N., and I. A. Renfrew (2009), Aircraft-based observations of air-sea fluxes over Denmark Strait and the Irminger Sea during high wind speed conditions, *Q. J. R. Meteorol. Soc.*, *135*(645), 2030–2045.
Petersen, G. N., I. A. Renfrew, and G. W. K. Moore (2009), An overview of barrier winds off southeastern Greenland during the Greenland flow distortion experiment, *Q. J. R. Meteorol. Soc.*, *135*(645), 1950–1967.
Rasmussen, L. (1989), Greenland winds and satellite imagery, *Vejret-Dan. Meteorol. Soc.*, 32–37.
Renfrew, I. A., et al. (2008), The Greenland flow distortion experiment, *Bull. Am. Meteorol. Soc.*, *89*(9), 1307–1324.
Skamarock, W. C. (2004), Evaluating mesoscale NWP models using kinetic energy spectra, *Mon. Weather Rev.*, *132*(12), 3019–3032.
Straneo, F., G. S. Hamilton, D. A. Sutherland, L. A. Stearns, F. Davidson, M. O. Hammill, G. B. Stenson, and A. Rosing-Asvid (2010), Rapid circulation of warm subtropical waters in a major glacial fjord in east Greenland, *Nat. Geosci.*, *3*(3), 182–186.
Våge, K., T. Spengler, H. C. Davies, and R. S. Pickart (2009), Multi-event analysis of the westerly Greenland tip jet based upon 45 winters in ERA-40, *Q. J. R. Meteorol. Soc.*, *135*(645), 1999–2011.
van As, D., et al. (2014), Katabatic winds and piteraq storms: Observations from the Greenland ice sheet, *Geol. Surv. Den. Greenl. Bull.*, *31*, 83–86.